



**HAL**  
open science

# Thermodynamic study of clathrates hydrates from hydrocarbon gas mixtures Consequences for capture CO<sub>2</sub> and flow assurance

Baptiste Bouillot, Quang-Du Le, Duyen Le Quang, Jean-Michel Herri

► **To cite this version:**

Baptiste Bouillot, Quang-Du Le, Duyen Le Quang, Jean-Michel Herri. Thermodynamic study of clathrates hydrates from hydrocarbon gas mixtures Consequences for capture CO<sub>2</sub> and flow assurance. Scientific conference on Oil Refining & Petrochemical Engineering ORPE 2014, Hanoi University of Mining and Geology, Oct 2014, Hanoi, Vietnam. pp. 151 à 167. hal-01104836

**HAL Id: hal-01104836**

**<https://hal.science/hal-01104836v1>**

Submitted on 19 Jan 2015

**HAL** is a multi-disciplinary open access archive for the deposit and dissemination of scientific research documents, whether they are published or not. The documents may come from teaching and research institutions in France or abroad, or from public or private research centers.

L'archive ouverte pluridisciplinaire **HAL**, est destinée au dépôt et à la diffusion de documents scientifiques de niveau recherche, publiés ou non, émanant des établissements d'enseignement et de recherche français ou étrangers, des laboratoires publics ou privés.

# Thermodynamic study of clathrate hydrates from hydrocarbon gas mixtures Consequences for capture CO<sub>2</sub> and flow assurance

BOUILLOT Baptiste<sup>1</sup>, LE QUANG Du<sup>1</sup>, LE QUANG Duyen<sup>2</sup>, HERRI Jean-Michel<sup>1</sup>.

<sup>1</sup>Gas Hydrate Dynamics Centre, Ecole Nationale Supérieure des Mines de Saint-Etienne, 158 Cours Fauriel, 42023 Saint-Etienne, France,

<sup>2</sup>Hanoi University of Mining and Geology

## Abstract

*This work is a contribution to the global understanding of the coupling between kinetics and thermodynamics to explain the composition of the clathrate hydrates during their crystallization from an aqueous liquid and a hydrocarbon gas phase. In this work, we face new experimental facts that open questioning after comparing the classical modeling of clathrate hydrates following the approach of [1] with our experimental data following a new procedure allowing determining the hydrate composition during crystallization and at equilibrium.*

*In this paper, we present details on the experimental procedure to measure the composition of the hydrate that crystallizes from a hydrocarbon gas mixture. We show that the results are time dependent and tend to thermodynamic equilibrium as time tends to infinity.*

*An immediate consequence concerns two major domains of applications, CO<sub>2</sub> capture from power plants, as well as flow assurance in the oil and gas industry. In fact, in both the cases, the crystallization is under non equilibrium conditions, and we conclude here that it necessarily leads to the formation of hydrates with a composition which is not predicted by classical modeling.*

**Keywords:** *Thermodynamics, Clathrate hydrates, CO<sub>2</sub> capture, Flow assurance.*

## 1. Introduction

### 1.1. Context

The offshore extraction of petroleum in deeper conditions increases day after day and favors the conditions of hydrate formation (low temperature and high pressure).

Hydrates are ice-like structures; formed by a process of crystallization, due to the union of water molecules around a “guest molecule”, in our case a gas molecule. When they form in the pipeline, they often lead to large pressure drops and in some cases to an impermeable plug, representing a great concern in flow assurance.

There are some methods used to deal with the hydrate formation. The most common among them is the use of thermodynamic hydrate inhibitors (THIs), which act on the hydrate equilibrium conditions, shifting it to higher pressure and lower temperature. The proportion of THIs injected is designed from the necessary shift to prevent hydrate formation, and the quantities of THI can be too much important and in consequence costly. Therefore, the researchers are urged to find other ways to handle the problem. Thus the focus changed from preventing the hydrate formation, and moved

to avoiding the pipeline blockage, by the use of low dosage hydrate inhibitors (LDHIs) including kinetic hydrate inhibitors (KHIs) and anti-agglomerates (AAs). The first acts by delaying or slowing the first steps of the crystallization (nucleation and growth), and the second works by preventing agglomeration then acting as dispersant.

As an oil/gas field matures, the fraction of water increases. Another parameter comes into play, since the cost of THIs injection is increased and the benefit of LDHIs is not well known. The development of new hydrate management strategies is limited by the understanding of hydrate plug formation mechanism. Also, the system, where the oil is the dispersed phase (oil-in-water emulsion), is poorly studied. Therefore, exploring the hydrate formation at high water cut shows a real interest, both at the level of the description of the crystallization itself as well as of the population level, but also at the crystal size level to describe its composition. We need first to describe the population level to understand the different mechanism of nucleation, growth and agglomeration under flowing (Figure 1) in order to design the type of additive to inject [2, 3]. After choosing the type of additive to delay or to prevent the crystallization, one needs to evaluate the quantity of additive to inject, and this quantity is dependent on the maximum quantity of hydrate that can be formed. The quantity of hydrates that can be formed can be estimated from a mass balance and depends on the estimation of the hydrate composition. In this work we focus on the fact that the hydrate composition could not be estimated directly from flash calculation implementing thermodynamic equilibrium calculation. In fact, in this work, we show that crystallization occurs under non equilibrium conditions giving hydrate with a composition different from equilibrium.

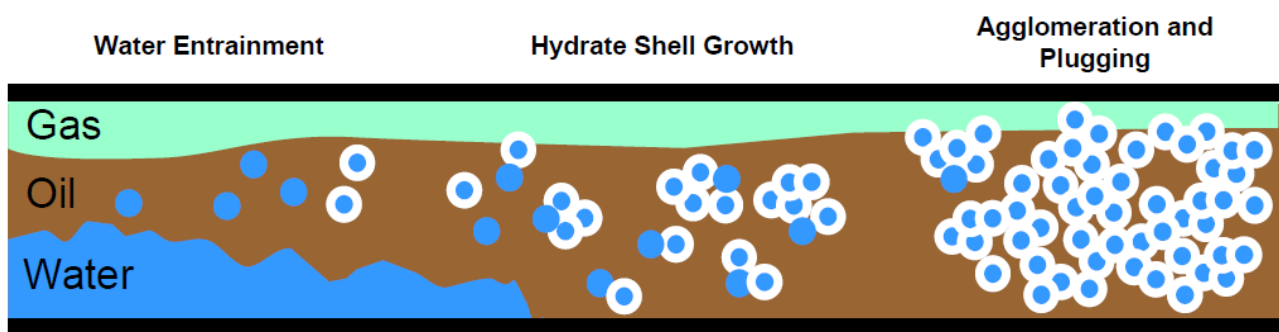


Figure 1: conceptual picture for hydrate formation in water-in-oil (W/O) emulsions. There are two critical interrelated steps in the formation of a plug: hydrate (shell) growth and hydrate agglomeration. Upon nucleation, a hydrate film rapidly forms around the water droplets. After the film has formed completely, the growth rate transition from a heat transfer limited process to a process limited by mass transfer. Hydrate forming gas molecules (guest) initially dissolved inside the water droplet can migrate to the hydrate film. At longer timescales the hydrate formation rate is limited by the mass transfer of the water or guest molecule through the hydrate film [4]. Once formed, it is assumed that the hydrate particles remain in the oil phase.

Another consequence of the non-equilibrium crystallization concerns a domain of application relative to gas separation and especially CO<sub>2</sub> capture [5]. In the capture process considered here,

CO<sub>2</sub> is physically adsorbed in solid gas hydrate crystals, rather than chemically bonded to a solvent such as in the amine process. Since the two main constituents of power station flue gasses, N<sub>2</sub> and CO<sub>2</sub> are both known to form gas hydrates with water at low temperatures and high pressures, a mixed hydrate containing H<sub>2</sub>O, N<sub>2</sub> and CO<sub>2</sub> is expected to form. From our experimental data, we observed pure CO<sub>2</sub> can form. The selectivity towards CO<sub>2</sub> in the mixed hydrate is dramatically enhanced in a way which cannot be explained by thermodynamic, but only from kinetic [6].

### 1.2. Clathrate hydrates

Gas clathrate hydrates, hereafter named gas hydrates, are ice like, solid inclusion bodies of hydrogen bonded water and small guest molecules. Hydrogen bonded water clusters may form cavities, where small guest molecules are encapsulated. The three most commonly occurring hydrate crystal structures are; structure I (sI), structure II (sII) and structure H (sH). The three structures are formed by a total of five different water cavities, the 5<sup>12</sup>, 5<sup>12</sup>6<sup>2</sup>, 5<sup>12</sup>6<sup>4</sup>, 5<sup>12</sup>6<sup>8</sup> and the 4<sup>3</sup>5<sup>6</sup>6<sup>3</sup> [7, 8]. A schematic of these cavities may be found in (Figure 2). The physical properties of the hydrate cavities and unit cells are provided in (Table 1). In its pure form, the unit cell of the sI hydrate contains two small 5<sup>12</sup> and six large 5<sup>12</sup>6<sup>2</sup> cavities while a unit cell of the sII hydrate contains sixteen small 5<sup>12</sup> and eight large 5<sup>12</sup>6<sup>4</sup> cavities. Both of these unit cell lattice structures belong to the cubic type. The sH hydrate structure is more complex and contains three 5<sup>12</sup>, two 4<sup>3</sup>5<sup>6</sup>6<sup>3</sup> and one 5<sup>12</sup>6<sup>8</sup> cavities [9]. This hydrate structure forms a hexagonal unit cell.

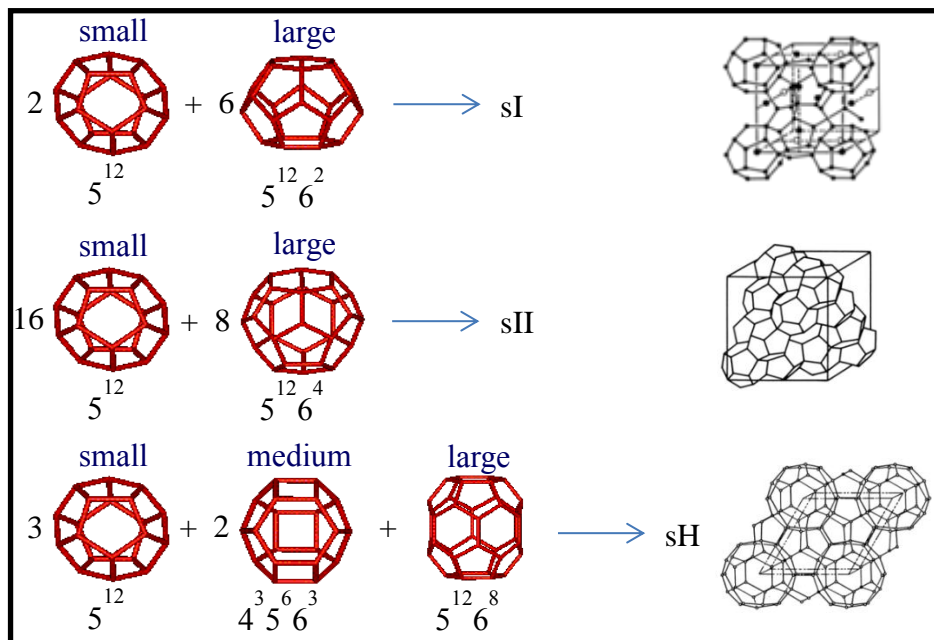
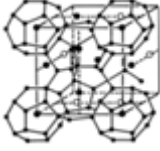
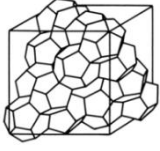
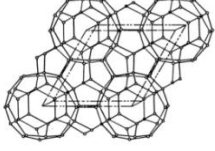


Figure. 2: Water molecules forming cages corresponding to hydrate structures, sI, sII and sH.

**Table1.** Clathrate hydrate structures [10]

Clathrate hydrate structures	S <sub>I</sub>		S <sub>II</sub>		S <sub>H</sub>		
							
Cavity	Small	Large	Small	Large	Small	Medium	Large
Description	5 <sup>12</sup>	5 <sup>12</sup> 6 <sup>2</sup>	5 <sup>12</sup>	5 <sup>12</sup> 6 <sup>4</sup>	5 <sup>12</sup>	4 <sup>3</sup> 5 <sup>6</sup> 6 <sup>3</sup>	5 <sup>12</sup> 6 <sup>8</sup>
Number per unit cell ( $m_j$ )	2	6	16	8	3	2	1
Average cavity radius (Å)	3,95	4,33	3,91	4,73	3,91 <sup>c</sup>	4,06 <sup>c</sup>	5,71 <sup>c</sup>
Coordination number <sup>a</sup>	20	24	20	28	20	20	36
(a)The number of oxygen atom per cavity							

A given hydrate structure is typically determined by the size and shape of the guest molecule. Each cavity may encapsulate one or in rare cases more guest molecules of proper sizes. It is the presence of the guest molecule that stabilizes the crystalline water structure at temperatures well above the normal freezing point.

## 2. Thermodynamic modelling: state of the art

In the case of hydrates, the thermodynamic equilibrium is the equality of chemical potentials of water in the liquid phase and in the hydrate phase. This relationship can be rewritten by introducing reference states. For the hydrate, the reference state used in the van der Waals and Platteeuw model is a hypothetical phase  $\beta$  which corresponds to the empty cavities hydrate. The equilibrium equation is then

$$\Delta\mu_w^{H-\beta} = \Delta\mu_w^{L-\beta} \quad (1)$$

Where  $\Delta\mu_w^{H-\beta}$  and  $\Delta\mu_w^{L-\beta}$  are the differences of the chemical potentials between water in hydrate or liquid phase and water in the reference state, respectively.  $\Delta\mu_w^{H-\beta}$  is then determined from statistical thermodynamics, whereas  $\Delta\mu_w^{L-\beta}$  is determined by means of relations from classical thermodynamics.

### Modeling of $\Delta\mu_w^{L-\beta}$

$$\Delta\mu_w^{H-\beta} = RT \sum_i v_i \ln \left( 1 - \sum_j \theta_j^i \right) \quad (2)$$

In Eq (2).  $v_i$  is the number of cavities of type  $i$  per mole of water (see Table 1) and  $\theta_j^i$  is the occupancy factor ( $\theta_j^i \in [0,1]$ ) of the cavities of type  $i$  by the gas molecule  $j$ . This last parameter is very important to define the thermodynamic equilibrium and to determine the hydrate properties.

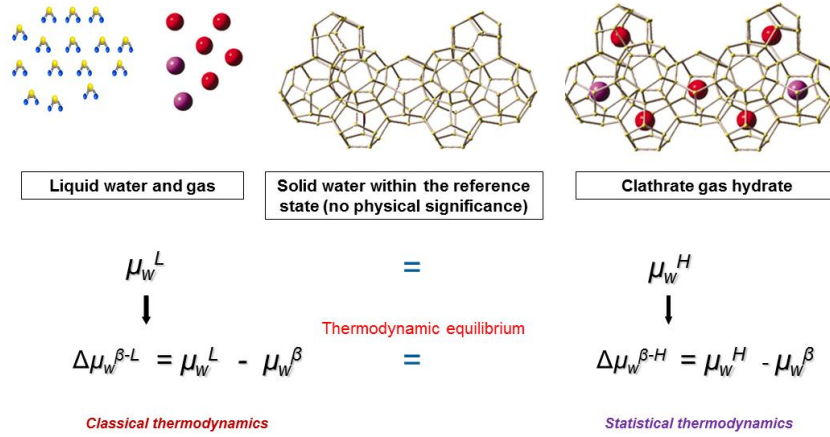


Figure 3 : Schematic of the equilibrium between the clathrate hydrate phase and the liquid phase using a reference state.

### Modeling of $\Delta\mu_w^{\varphi-\beta}$

The chemical potential of water in the aqueous phase is calculated by means of the Gibbs-Duhem equation of classical thermodynamics which expresses the variation of the free enthalpy with temperature, pressure and composition. The reference conditions are the temperature  $T_0 = 273.15$  K and the pressure  $P_0 = 1$  bar. The difference of the chemical potential of water between the reference phase (liquid in our case, but it could be ice or vapour phase) and the (hypothetical) empty hydrate phase  $\beta$ ,  $\Delta\mu_w^{\varphi-\beta}$ , can be written as follows:

$$\Delta\mu_w^{L-\beta} = T \frac{\Delta\mu_w^{L-\beta}|_{T^0, P^0}}{T^0} - T \int_{T^0}^T \frac{\Delta h_w^{L-\beta}|_{P^0}}{T^2} dT + \int_{P^0}^P \Delta v_w^{L-\beta}|_t dP - RT \ln a_w^L|_{T, P} \quad (3)$$

The activity of water in the liquid phase,  $a_w^L$ , is given as the product of the mole fraction of water in the liquid phase,  $x_w$ , and the activity coefficient of water,  $\gamma_w^L$ , hence  $a_w^L = x_w \gamma_w^L$ . In a good approximation, the aqueous phase (this work) can be regarded as ideal and the activity coefficient therefore can be set to unity, resulting in  $a_w^L \cong x_w$ . However, in the presence of polar molecules, or salts, the system usually shows strong deviations from ideality and  $\gamma_w^L$  needs an appropriate description, for example using eNTRL model [11].

The value of  $\Delta v_w^{L-\beta}|_T$  is a first order parameter. It has been measured with high accuracy by [12] from X ray diffraction. Since that data is believed to be very reliable, the parameter  $\Delta v_w^{L-\beta}|_T$  in our model calculations has been taken from this source.

The value of  $\Delta h_w^{L-\beta}|_{P^0}$  is a first order parameter as well. A refinement of the model is given by [7, 8] that takes into account the temperature dependence of  $\Delta h_w^{L-\beta}|_{P^0}$  using the well-known classical thermodynamic relationship

$$\Delta h_w^{L-\beta}|_{P^0} = \Delta h_w^{L-\beta}|_{T^0, P^0} + \int_{T^0}^T \Delta C_{P,w}^{L-\beta}|_{P^0} dT \quad (4)$$

Assuming a linear dependence of  $\Delta C_{P,w}^{L-\beta}|_{P^0}$  on temperature according to:

$$\Delta C_{P,w}^{L-\beta}|_{P^0} = \Delta C_{P,w}^{L-\beta}|_{T^0, P^0} + b_{P,w}^{L-\beta} (T - T^0) \quad (5)$$

The model becomes first order dependent on  $\Delta h_w^{L-\beta}|_{T^0, P^0}$  (hereafter referred as  $\Delta h_w^{L-\beta,0}$ ) and second order dependent on  $\Delta C_{P,w}^{L-\beta}|_{T^0, P^0}$  (hereafter abbreviated as  $\Delta C_{P,w}^{L-\beta,0}$ ) and  $b_{P,w}^{L-\beta}$ . The last first order parameter of the equation is  $\Delta \mu_w^{L-\beta}|_{T^0, P^0}$  (hereafter referred to as  $\Delta \mu_w^{L-\beta,0}$ ) The values of  $\Delta \mu_w^{L-\beta}|_{T^0, P^0}$  (here after called  $\Delta \mu_w^{L-\beta,0}$ ),  $\Delta h_w^{L-\beta,0}$ ,  $\Delta v_w^{L-\beta}|_T$ ,  $\Delta C_{P,w}^{L-\beta,0}$  and  $b_{P,w}^{L-\beta}$  have been detailed by [7]. A special attention has been given by us to the values of  $\Delta \mu_w^{L-\beta,0}$  and  $\Delta h_w^{L-\beta,0}$  [7] has reported different values from different authors, and he retained the data from [13]. From our work [10], from fitting from experimental data about the CO<sub>2</sub>-N<sub>2</sub>-CH<sub>4</sub> hydrate equilibrium, we prefer now to work with the values from [14], given in [10].

### 3. Experimental procedure and set-up

#### 3.1. Experimental set-up

The apparatus used for this study is presented in Figure 4. This experimental set-up is mainly composed of an instrumented batch reactor (Autoclave, 2.36 L). This reactor was fed with pure gas, or prepared gas mixture. A HPLC pump (JASCO-PU-1587) allowed the liquid injection (water + LiNO<sub>3</sub> as tracers for determining by mass balance the amount of aqueous phase in the cell at each step). A cryostat (HUBERT CC-505) allowed the temperature control with 0.02°C accuracy, and two sapphire windows (12cm x 2cm) are placed on each sides of the reactor to survey the inside. The reactor was stirred on both upper side (vapor phase) and lower side (liquid/hydrate phase). The pressure, and the temperature on both upper/lower side, were monitored online by a pressure sensor (0.1 bar accuracy) and a temperature sensor (Pt 100, 0.02 °C accuracy), with the help of a data acquisition system.

To be able to determine the composition of each phase at the equilibrium, the gas phase composition was monitored online using a gas chromatograph (VARIAN model CP-3800 GC with



a 50m PORA BOND Q column). A ROLSI injector was used for the sampling (a few  $\mu\text{m}^3$  each sample), and Helium was used a carrier gas. The liquid phase could be analyzed offline by ionic chromatography (DIONEX ionic exchange chromatograph). A valve allowed the sampling of the liquid phase (water +  $\text{LiNO}_3$ ) with the help of the inner pressure of the reactor.

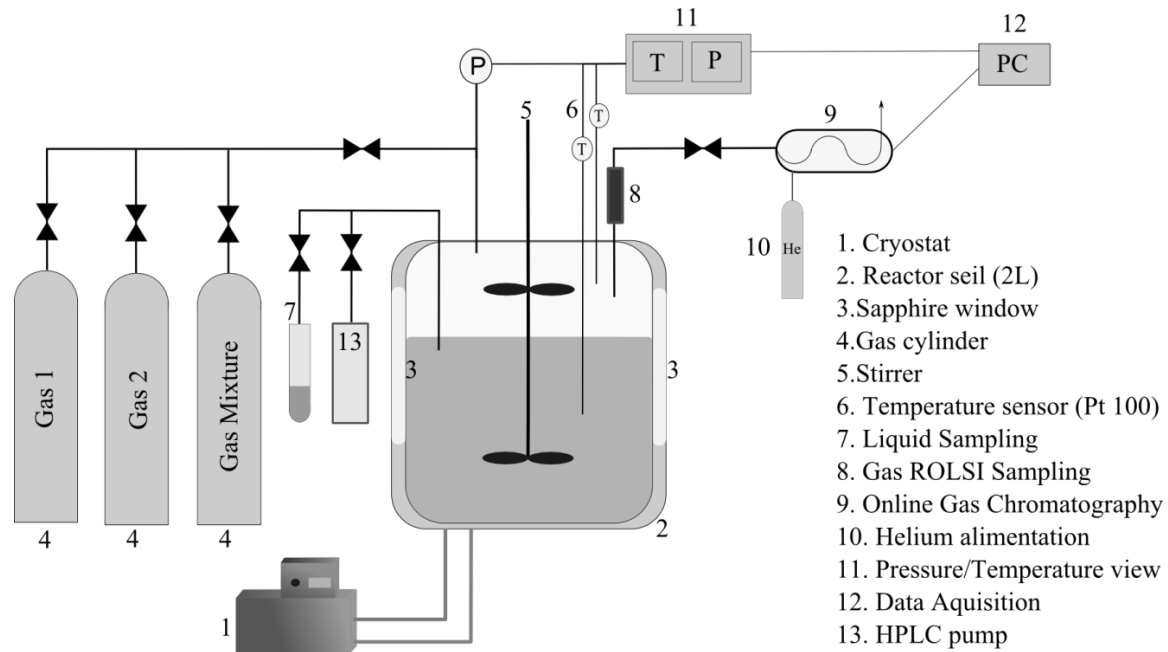


Figure 4 : Experimental set-up

### 3.2. Experimental procedure at high crystallization rate

The first experimental procedure was the same as in our previous studies on gas hydrates equilibrium [10]. In this procedure, the crystallization occurred at a “high rate” (or at a high supersaturation). At first, the reactor was cleaned and vacuum is made (for 40÷50 minutes). Then, the cell was filled with the desired composition either by direct injection of the various components or from a bottle where the mixture has been prepared.

The pressure was measured, and the temperature was set to  $1^\circ\text{C}$  (internal regulation of the cryostat). The gas composition in the cell is checked with GC analysis before any measurement.

A 10 mg/L water mixture of  $\text{LiNO}_3$  was prepared and injected (about 800÷1000g) into the reactor thanks to the HPLC pump (n°13). The used water was ultrapure water (first category,  $18.2 \text{ M}\Omega\cdot\text{cm}$ ). A rise in the pressure, due to the added volume of liquid, was observed. Then, the reactor was stirred at the rate of 450 rpm, on both upper side, and lower side. The gas was charged into the liquid phase, and after some time (induction time), the crystallization begins. Due to the exothermicity of the reaction, a brief rise in temperature was observed. At this point, we waited for the equilibrium to be reached (no more temperature/pressure evolution). This took about 2 to 4 days depending on the mixture and initial pressure. When the equilibrium was reached, a sample of the gas phase was taken and injected into the gas chromatograph to determine the molar composition. A liquid sample was also taken to be analyzed *offline* by ionic chromatography (about 4.5÷5.5mg).



Then, the dissociation of the hydrate was started. The temperature was increased by about 1.5°C. When the new equilibrium was reached (24h), new samples of the fluid phases are taken. Then, the process was repeated until there was no longer a hydrate phase in the reactor. The whole procedure is summarized on Figure 5 and 6.

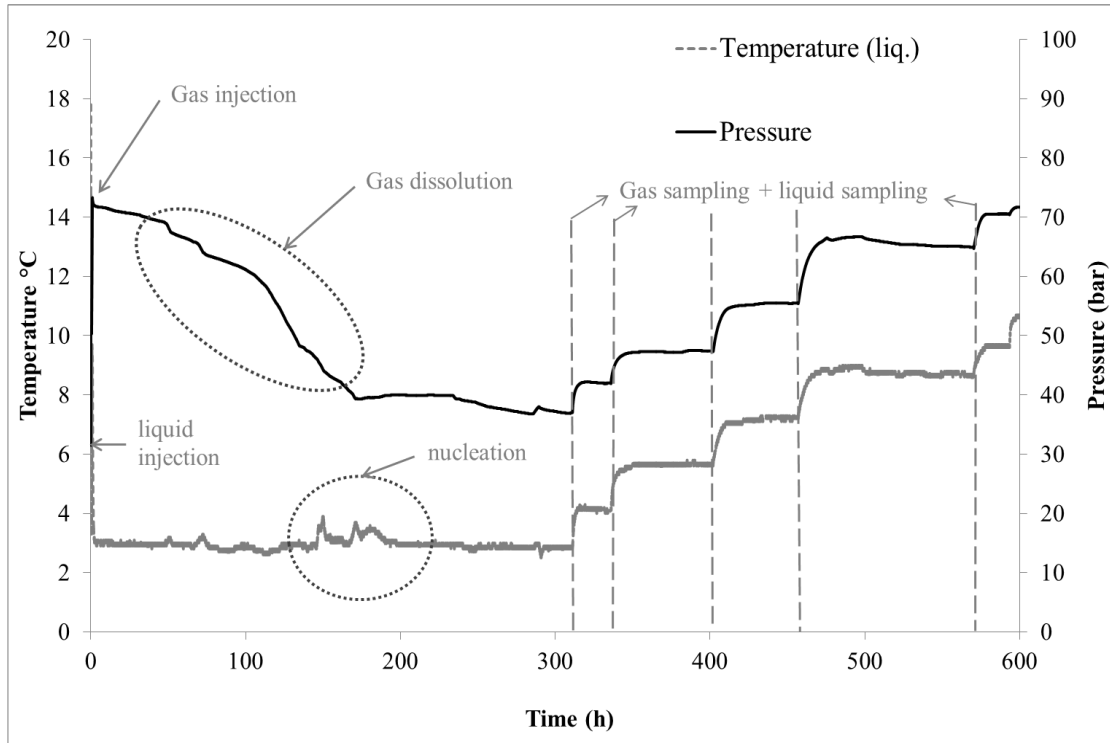


Figure 5: Pressure – Temperature evolution during equilibria experiments at high crystallization rate.

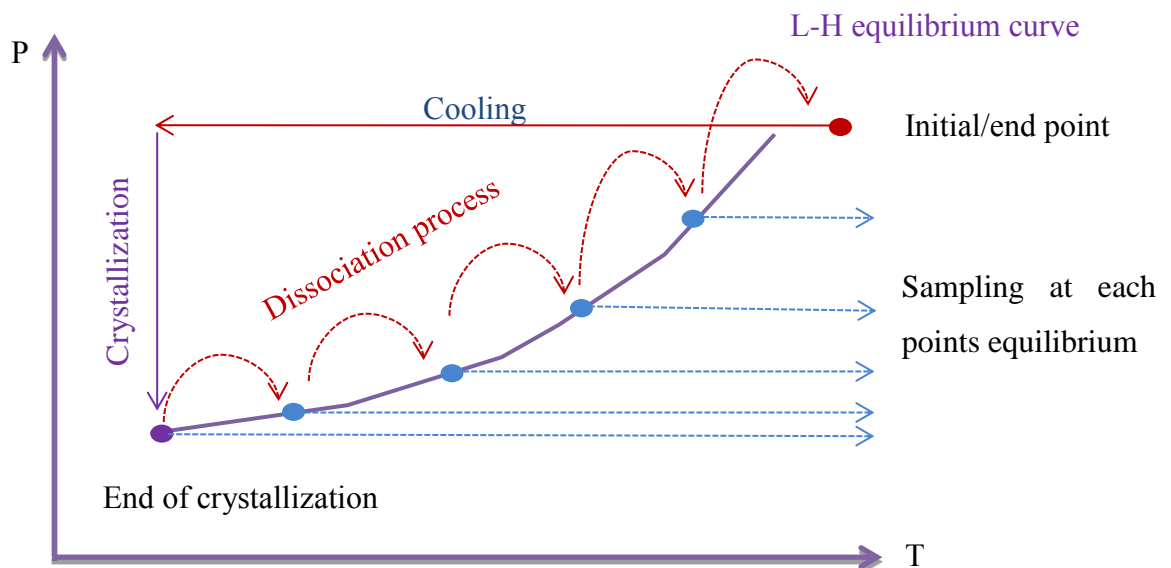


Figure 6: Pressure – Temperature evolution during equilibria experiments at high crystallization rate.

### 3.3. Experimental procedure at low crystallization rate

In this second procedure, the objective is to focus on thermodynamic equilibrium avoiding as much as possible any kinetic effect. In this procedure, the crystallization rate should be closer to the hydrate formation process in pipelines at steady state (constant evolution of the pressure and of the temperature along the pipes). The objective is to stay as close as possible to the thermodynamic equilibrium curve, in order to decrease the kinetic effect on crystallization.

The pressure/temperature evolution as function of the time for the only experiment with this procedure is shown on Figure 3. Instead of decreasing very quickly the temperature to the final point (between 0 and 2°C), the crystallization occurred close to the initial point in the hydrate free area. Then, the temperature was decreased very slowly (about 0.1 ÷ 0.3 °C per day). Every a decreased of 1°C samples of the gas and liquid phases were taken and analyzed. This procedure concerns only the gas mixture n°12.

In the next section, it is explained which the studied mixtures are, and how they have been prepared.

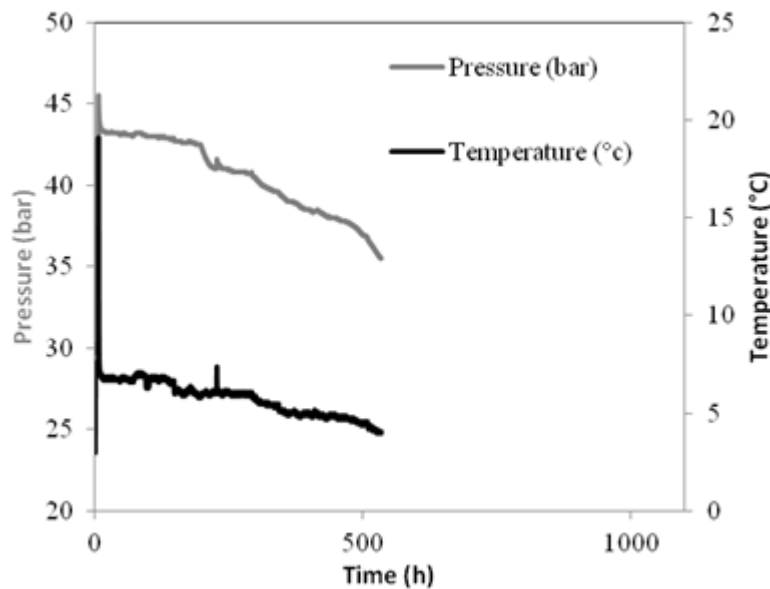


Figure 7. Pressure – Temperature evolution during equilibrium experiment at low crystallization rate.

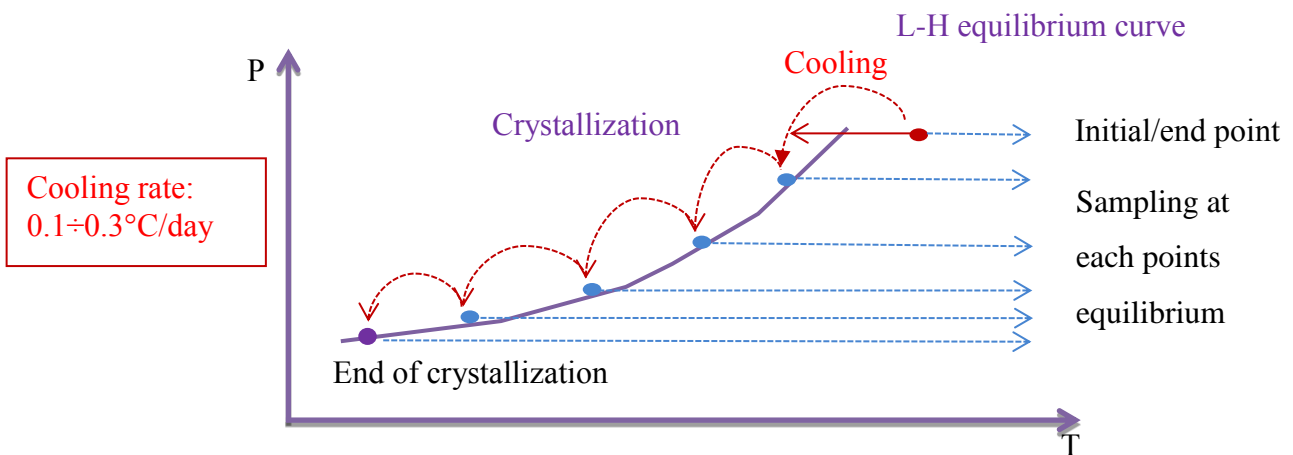


Figure 8 : Pressure – Temperature evolution during equilibria experiments at low crystallization rate

### 3.4. Mass balance calculation

At given values of the state variables, a gaseous, a liquid and a solid hydrate phases are present in the system the initial quantity of the gases in the reactor is distributed between these three phases. Thus, in equilibrium, the quantity of gas in the hydrate phase can be determined from a mass balance according to:

$$n_{i,0}^{initial} = n_i^G + n_i^L + n_i^H \quad (6)$$

Where  $n_{i,0}^{initial}$  is the mole number of the gases injected into reactor, and  $n_i^G, n_i^L, n_i^H$  are the mole numbers of the gaseous component  $i$  ( $i$ : CO<sub>2</sub>, N<sub>2</sub>, hydrocarbon) in the hydrate, the liquid and the gas phase, respectively.

The amount of substance of the gases dissolved in the liquid phase is then estimated by means of corresponding gas solubility data, whereas the mole number of the gases present in the gas phase is calculated by using an equation of state approach as outlined in the next sections.

#### 3.3.1. Calculation of compressibility index

The compressibility factor in the gas phase in any equilibrium state can be calculated by means of the classical Eq.(7) combined with means of a suitable equation of state (EOS), e.g., a classical cubic EOS. For the data evaluation in this study, the Soave-Redlich and Kwong (SRK) and (EOS) equation has been used parameters from [15].

$$Z(T, P, \vec{y}) = \frac{PV}{nRT} \quad (7)$$

With respectively  $n \equiv n^G$  (at each situation) and in Eq. (7),  $T$ ,  $P$ , and  $V$  are the temperature, pressure and total volume, respectively, while  $\vec{y} = (y_1, \dots, y_N)$ ,  $n$  and  $R$  represent the vector of the mole fractions of the components in the mixture, the total mole number in the gas mixture, and the universal gas constant.

#### 3.3.2. Composition of the gases initial inside reactor

Before injecting water inside reactor, at homogeneous and stability gases mixtures, the mole fraction of each gas in the gas phase  $x_j$  ( $j$  is CO<sub>2</sub>, N<sub>2</sub>, hydrocarbon) is determined by using gas chromatography analysis (\*).

We recall here that the reactor of total inner volume  $V_R = 2.44$  (liter) is initially filled with the gaseous components at the initial temperature  $T_0$  and under the initial total pressure  $P_0$ .

$$n_0^G = \frac{P_0 V_R}{Z(T, p, y_{j,0}) R T_0} \quad (8)$$

Utilizing the results from (\*) means that the system consists of a gas phase only, being composed of the gases components  $j$ , each of which having the initial mole fractions  $x_j$  ( $j$  is CO<sub>2</sub>, N<sub>2</sub>, hydrocarbon). Combine with the measurements of temperature, pressure, and the compressibility factor in the gas phase, the initial total mole number in the gas phase  $n_0^G$  is derived from Eq. (8). Then, we obtain mole number of each gas in initial situation.

### 3.3.3. Composition of the gases solubility in liquid phase

#### a) The volume of the aqueous phase:

As mentioned above, the liquid phase contains LiNO<sub>3</sub> as a tracer. Initially the concentration of lithium  $[Li^+]_0$  and the initial volume of liquid  $V_0^L$  are known. During the crystallization and dissociation steps, the concentration of lithium is measured by ion-exchange chromatography after sampling. So, we can calculate the volume of liquid water from a mass balance for the Li<sup>+</sup> ions:

$$V_0^L [Li^+]_0 = V^L [Li^+] \Rightarrow V^L = \frac{V_0^L [Li^+]_0}{[Li^+]} \quad (9)$$

Where  $V^L$  and  $[Li^+]$  are the volume of the liquid aqueous phase and the molar concentration of lithium in this phase, i.e., in the sample, corresponding to a given step of the crystallization or dissociation.

#### b) The mole fraction of gases dissolved in liquid phase [16]

The solubility of a gas in a liquid is determined by the equations of phase equilibrium. If a gaseous phase and a liquid phase are in equilibrium, then for any component  $i$  the fugacity in both phases must be the same:

$$f_i^L = f_i^V \quad (10)$$

The mole number of gas in the liquid phase Eq. (10) is calculated in a good approximation by using solubility data of the gas in water [17] under the assumption that LiNO<sub>3</sub>, due to its low concentration (10 ppm), does not affect this solubility.

*For the solving equilibrium, there are two different approaches:*

**The classical or unsymmetrical approach**, called  $\gamma\text{-}\phi$ , which consists of choosing an equation of state (EOS) for the gas phase and a solution model for the liquid phase

$$\phi_i^v y_i^v P = \gamma_i x_i f_i^{0L} \quad (11)$$

The fugacity of the pure liquid components  $f_i^{0L}$  is expressed as function of the saturated vapor pressure of the liquid

$$f_i^{0L} = P_i^{sat} \phi_i^0(T, P_i^{sat}) \exp\left(\frac{v_i^L (P - P_i^{sat})}{RT}\right) \quad (12)$$

$v_i^L$  is the molar volume of the pure liquid component  $i$  ( $i = \text{solvent}$ ) at saturation. The exponential term is called Poynting correction factor. It represents the deviation between the saturated vapor pressure of component  $i$  and the equilibrium pressure.

**The symmetric approach**, called ( $\phi^v = \phi^L$ ), consists in describing the gas phase and the liquid phase in terms of equations of state (EOS) along with appropriate mixing rules

$$\phi_i^v \gamma_i^v = \phi_i^L x_i^L \quad (13)$$

For treating the gas solubility, the unsymmetrical approach is combined with the unsymmetrical convention, which corresponds to infinite dilution reference (i.e. the activity coefficients of the gas molecules into the water equal to unity). The equilibrium condition reads:

$$\phi_i^v \gamma_i^v P = \gamma_i x_i H_i \quad (14)$$

where  $H_i$  is Henry's law constant. It is expressed by means of the relation

$$H_i = H_{i,Psat} \exp\left(\frac{v_i^\infty (P - P_i^{sat})}{RT}\right) \quad (15)$$

The so-called solubility models enable the calculation of Henry's law constant. It has to be reminded that the Henry's law constant is determined at the saturated vapour pressure of the pure solvent ( $H_{i,Psat}$ ). Thus, the Poynting factor corrects for the pressure difference between  $P_{sat}$  of the pure solvent (here is the water) and the system pressure  $P$ . The partial molar volume of the gas  $i$  at infinite dilution ( $v_i^\infty$ ) can be calculated from a correlation proposed by [18]. However, it is fixed here to  $32 \text{ cm}^3 \cdot \text{mol}^{-1}$  for the majority of the components.

[17] Proposed the following correlation for Henry's constant with temperature

$$H_{i,Psat} = \exp\left(A + \frac{B}{T}\right) \quad (16)$$

The coefficients  $A$  and  $B$  are compiled in [Table 2](#). The temperature is expressed in Kelvins and Henry's constant is given in atmospheres.

Table 2: Constants for calculating Henry's constant [17]

Gas	A	B	$v_i^\infty$ (Cm <sup>3</sup> /mole)
CH <sub>4</sub>	15.826277	-1559.0631	32
C <sub>2</sub> H <sub>6</sub>	18.400368	-2410.4807	32
C <sub>3</sub> H <sub>8</sub>	20.958631	-3109.3918	32
CO <sub>2</sub>	14.283146	-2050.3269	32
N <sub>2</sub>	17.934347	-1933.381	32

**c) The mole number of gases in the liquid phase:**

The mole number of a gas in a liquid is determined by the Eq. (17) and the mole number of liquid ( $n_{water}^L$ ) is known.

$$x_i = \frac{n_i}{n_i + n_j + n_{water}^L} \quad (17)$$

Because, the very good approximations  $n_i$  and  $n_j \ll n_{H_2O}^L$ , and  $V^L \cong V_w^L$ . Therefore, in this case, we can be considered the values  $n_i = 0$  during the time calculate  $n_j$  and vice versa.

**3.3.4. Composition of the gases in gas phase**

Eq. (7) has also been used to determine the total amount of the gas phase in a state corresponding to the three phase hydrate-liquid-vapor equilibrium. In the latter case, the initial values of the variables are to be replaced by the corresponding values measured in that equilibrium state, i.e,  $T_0$ ,  $P_0$ ,  $y_{j,0}$  and  $n_0^G$  are to be substituted for  $T$ ,  $P$ ,  $y_j$  and  $n^G$ . The volume of the reactor  $V_R$  has been replaced by the actual value of the gas phase  $V^G$ , which for any given equilibrium state has been approximated by:

$$V_{gas\ phase}^{Gas} = (V_{reactor} + V_{sample\_liq}^{water}) - V_{inject}^{water} \quad (18)$$

Utilizing the results from the gas chromatographic analysis we have mole fraction of each gas in composition ( $x_i^{eq}$ ). Combine  $V_{Gas\_phase}^{Gas}$  and ( $x_i^{eq}$ ) we can be calculated  $n_i^G$  by means of a suitable equation of state (EOS), and the Soave-Redlich and Kwong equation (SRK).

## 4. Results

**Table 3:**  $CO_2-N_2$  Clathrate Hydrate equilibrium data. The simulation curve is obtained with the GasHyDyn simulator and compared with the Experimental Equilibrium Data (High crystallization rate)

Experimental Equilibrium Data						GASHYDYN Prediction			
T	P	Gas composition		Hydrate composition		Structure	P	Hydrate composition	
(°C)	(MPa)	$x_{CO_2}$	$x_{N_2}$	$x_{CO_2}$	$x_{N_2}$		(MPa)	$CO_2$	$N_2$
2.3	2.46	0.667	0.333	0.971	0.029	SI	2.53	0.955	0.045
3.1	2.6	0.689	0.311	0.979	0.021	SI	2.69	0.958	0.042
3.3	2.66	0.699	0.301	0.978	0.022	SI	2.73	0.960	0.040
4.3	2.87	0.723	0.277	0.975	0.025	SI	2.99	0.962	0.038
5.2	3.13	0.747	0.253	0.974	0.026	SI	3.22	0.966	0.034
6.0	3.38	0.768	0.232	0.971	0.029	SI	3.48	0.968	0.032
Mean Deviation (%)							<b>%D=3.1</b>	<b>%D=1.04</b>	<b>%D=24.7</b>

**Table 4:**  $CO_2-CH_4-C_2H_6$  Clathrate Hydrate equilibrium data. The simulation curve is obtained with the GasHyDyn simulator and compared with the Experimental Equilibrium Data (High crystallization rate)

Experimental Equilibrium Data					GASHYDYN Prediction				
T	P	Hydrate composition			Structure	P	Hydrate composition		
(°C)	(MPa)	$CO_2$	$CH_4$	$C_2H_6$		(MPa)	$CO_2$	$CH_4$	$C_2H_6$
2.75	3.54	0.144	0.769	0.087	SI	2.72	0.097	0.739	0.164
3.65	3.81	0.144	0.769	0.087	SI	2.90	0.103	0.717	0.180
5.15	4.23	0.141	0.774	0.085	SI	3.22	0.106	0.683	0.210
6.55	4.56	0.141	0.777	0.082	SI	3.64	0.107	0.669	0.224
7.80	5.12	0.135	0.777	0.089	SI	4.11	0.112	0.662	0.226
9.25	5.99	0.049	0.804	0.148	SI	4.83	0.127	0.661	0.211
Mean Deviation (%)						<b>%D=21.7</b>	<b>%D=48.18</b>	<b>%D=11.4</b>	<b>%D=119.2</b>

**Table 5:**  $CO_2-CH_4-C_2H_6$  Clathrate Hydrate equilibrium data. The simulation curve is obtained with the GasHyDyn simulator and compared with the Experimental Equilibrium Data (Low crystallization rate,  $0.1 \div 0.3$  °C/day)

Experimental Equilibrium Data					GASHYDYN Prediction				
T	P	Hydrate composition			Structure	P	Hydrate composition		
(°C)	(MPa)	$CO_2$	$CH_4$	$C_2H_6$		(MPa)	$CO_2$	$CH_4$	$C_2H_6$
-	3.775	0.066	0.851	0.083	SI	3.641	0.062	0.843	0.095
-	3.56	0.085	0.892	0.023	SI	3.512	0.061	0.846	0.093



-	3.18	0.061	0.894	0.045	SI	3.277	0.061	0.869	0.070
-	3.04	0.092	0.894	0.014	SI	3.033	0.059	0.871	0.070
-	2.76	0.071	0.899	0.030	SI	2.748	0.057	0.885	0.058
-	3.775	0.066	0.851	0.083	SI	3.641	0.062	0.843	0.095
Mean Deviation (%)						<b>%D=1,72</b>	<b>%D=18.0</b>	<b>%D=2.6</b>	<b>%D=173.14</b>

**Table 6:**  $CH_4$ - $C_3H_8$  Clathrate Hydrate equilibrium data. The simulation curve is obtained with the GasHyDyn simulator and compared with the Experimental Equilibrium Data (Low crystallization rate,  $0.1 \div 0.3$  °C/day)

Experimental Equilibrium Data						GASHYDYN Prediction			
T	P	Gas composition		Hydrate composition		Structure	P	Hydrate composition	
(°C)	(MPa)	xCH <sub>4</sub>	xC <sub>3</sub> H <sub>8</sub>	xCH <sub>4</sub>	xC <sub>3</sub> H <sub>8</sub>		(MPa)	xCH <sub>4</sub>	xC <sub>3</sub> H <sub>8</sub>
5,9	1,08	0,902	0,098	0,809	0,191	SI	-	-	-
4,8	0,94	0,905	0,095	0,815	0,185	SI	-	-	-
3,7	0,83	0,910	0,090	0,818	0,182	SI	-	-	-
2,6	0,72	0,912	0,088	0,823	0,177	SI	-	-	-
1,8	0,66	0,912	0,088	0,825	0,175	SI	-	-	-
0,9	0,59	0,914	0,086	0,827	0,173	SI	-	-	-
Mean Deviation (%)							<b>%D= -</b>	<b>%D= -</b>	<b>%D= -</b>

## 5. Discussion

The experimental results of CO<sub>2</sub> and N<sub>2</sub> gases mixtures (Table 3) can be regarded as a good case study at thermodynamic equilibrium. The equilibrium pressure is simulated with a precision of 3,1% and the composition of gas in the hydrate phase is simulated with a precision of 1,04 % for CO<sub>2</sub>, and of 24,7% for N<sub>2</sub> respectively.

In a way, this result is surprising when compared to other results presented in Tables 4÷6, because the experimental procedure was used here at high crystallization rate, and we can suspect a non-equilibrium formation regime.

In fact, having a look to Table 4, which gives results from an experiment at high crystallization rate also, but for a different gas mixture CO<sub>2</sub>-CH<sub>4</sub>-C<sub>2</sub>H<sub>6</sub>, we observe that neither the hydrate composition nor the pressure are at equilibrium (in accordance with simulated results).

So, it can be said that the crystallization performed at high driving force can or cannot form hydrate at equilibrium. It depends on the gas molecules.

To be sure that hydrates are formed at equilibrium, we show on Table 5 that it is necessary to use the experimental procedure at low driving force. In that case, the crystallization from the gas mixture CO<sub>2</sub>-CH<sub>4</sub>-C<sub>2</sub>H<sub>6</sub> gives a hydrate composition near from equilibrium, at a pressure which is

very well predicted by simulation also. The only exception is that the composition of  $C_2H_6$  which deviates from modeling is very high whatever the crystallization regime. In our understanding, we consider that bigger molecules such as ethane have a lower mobility in the liquid, and a lower solubility. It can give an enclathration rate which is not high enough to compete with the smallest molecules and/or the high soluble molecules enclathration rates.

In the last table (Table 7) gives the experimental results concerning the  $CH_4-C_3H_8$  gas mixture. The data are not compared to modeling because we did not retrieve the Kihara parameters of propane up to now, which are necessary to model the occupancy of cavities in the classical Van der Waals & Platteeuw model (1959) [1].

The determination of Kihara parameters is explained in detailed in [19] and [20]. It implies to extract from experimental data base a single gas equilibrium curve which covers a large enough temperature range. It is the case for  $N_2$ ,  $CO_2$ ,  $CH_4$ , and  $C_2H_6$ , but not  $C_3H_8$ .

For propane, the determination of Kihara parameters implies to extract from experimental data base, the gas mixture equilibrium data, for gases components (except propane) which the Kihara parameters are well known.

But, we need to be sure that the experimental data are really at equilibrium, and we open here a doubt about the difficulty to form a hydrate truly at equilibrium, even by waiting very long time during crystallization as we did for  $CO_2-CH_4-C_2H_6$  mixture without forming a hydrate for which  $C_2H_6$  composition is at equilibrium.

So, for us, at the moment, we are in a main difficulty to be sure to give experimental data in presence of propane at equilibrium. So we cannot propose a simulation in Table 6.

## 6. Conclusion

Gas hydrate equilibrium experiments of hydrocarbon gas mixtures ( $N_2-CO_2-CH_4-C_2H_6-C_3H_8$ ) were performed in an instrumented batch reactor. In this study, both classic pressure/temperature equilibrium data but also molar compositions (gas phase and hydrate phase) are given.

- The two procedures used (high and low crystallization rates) highlight the kinetic effect on hydrate formation. For example, the enclathration of the bigger molecule (ethane) is more important at low crystallization rate.
- In the end this work, a modeling part was not added since it is the subject of another work. In this other work, based on a kinetic consideration [6] there is a questioning about the validity of these measurements as thermodynamic measurements (but as kinetic measurements). This is why the present data were analyzed using a thermodynamic model in an in-house software to discuss the possibility to crystallize gas hydrate at thermodynamic equilibrium at a high crystallization rate [5].

## List of symbols

$P$	Pressure [Pa]
$T$	Temperature [K]
$V$	Volume [m <sup>3</sup> ]
$R$	Gas molecule equivalent radius [m] or universal gas constant [8.314472 m <sup>2</sup> kg s <sup>-2</sup> K <sup>-1</sup> mol <sup>-1</sup> ]
$Z$	Compressibility factor
$H_i$	Henry coefficient [ $H_i$ ] = Pa
$A$	Coefficient in correlating equation for Henry's law constant, and in Parrish and Prausnitz' equation, respectively
$B$	Coefficient in correlating equation for Henry's law constant [K <sup>-1</sup> ], and in the Parrish and Prausnitz relation, respectively
$\mu$	Chemical potential of a species or component, [ $\mu$ ] = J mol <sup>-1</sup>
$f$	Fugacity, [ $f$ ] = Pa
$\theta$	Fraction of sites occupied (by a particular species and for a specific type of cavity as indicated by additional subscripts, dimensionless
$x$	Mole fraction of a chemical species, dimensionless;
$v_i^L$	The molar volume of the pure liquid component $i$
$v_i^\infty$	The partial molar volume of the gas $i$ at infinite dilution
$\phi$	Coefficient of fugacity
$\gamma$	Activity coefficient [-]

## Acknowledgements

This work has been supported by the projects: iCap, SECOHYA, ACCACIA and TOTAL-Archimede.

Furthermore, the authors are grateful to all members of the GasHyDyn team for their constant support and to the technical staff members: Fabien Chauvy and Alain Lallemand.

## References

- [1] Van der Waals, J. H.; Platteeuw, J. C., «Clathrate solutions,» *Adv. Chem. Phys.*, vol. 2, pp. 1-57, 1959.
- [2] Hung Leba, Cameirao A., Herri, J.M., Darbouret, M., Peytavy, J.L., Glénat, P., «Chord length distributions measurements during crystallisation and agglomeration of gas hydrate in a water-in-oil emulsion: Simulation and experimentation,» *Chemical Engineering Science*, vol. 65, n° 13, pp. 1185-1200, 2010.
- [3] A. Cameirao, H. Le Ba, M. Darbouret, J.-M. Herri, J.-L. Peytavy, P. Glénat, "Chord length distributions interpretation using a polydispersed population: Modeling and experiments," *Journal of Crystal Growth*, vol. 342, no. 1, p. 65–71, 2012.
- [4] D. J. Turner, «PhD Thesis "Clathrate Hydrate Formation in Water-in-Oil Dispersions".,» Colorado School of Mines, Golden, CO 80401, United States, 2005.

- [5] Herri JM, Le Quang Duyen, Kwaterski M, Bouillot B, Glenat P, Duchet-Suchaux P, «How to explain the hydrate composition from CO<sub>2</sub>-C<sub>1</sub>-C<sub>2</sub>-C<sub>3</sub>-C<sub>4</sub> gas mixtures: toward a kinetic understanding versus thermodynamic and consequences on the evaluation of the kihara parameters,» chez *The 8th International Conference on Gas Hydrate (ICGH8)*, BEIJING, China, 2014.
- [6] Jean-Michel Herri, Matthias Kwaterski, «Derivation of a Langmuir type of model to describe the intrinsic growth rate of gas hydrates during crystallisation from gas mixtures,» *Chemical Engineering Science*, vol. 81, pp. 28-37, 2012.
- [7] E. Sloan, Clathrate hydrates of natural gases, 2nd ed. éd., New York: Marcel Decker, 1998.
- [8] E. Sloan. et C. Koh, Clathrate hydrates of natural gases, 3rd ed. éd., Boca Raton: CRC Press, 2008.
- [9] Sum, A.K. , Koh, C.A. , Sloan, E.D., *Ind. Eng. Chem. Res*, n° 148, p. 7457–7465, 2009.
- [10] J.-M. Herri, A. Bouchemoua, M. Kwaterski, A. Fezoua, Y. Ouabbas, A. Cameirao «Gas hydrate equilibria for CO<sub>2</sub>-N<sub>2</sub> and CO<sub>2</sub>-CH<sub>4</sub> gas mixtures—Experimental studies and thermodynamic modelling,» *Fluid Phase Equilibria*, vol. 301, n° 12, pp. 171-190, 2011.
- [11] Matthias Kwaterski, J.-M. Herri. «Modelling of gas clathrate hydrate equilibria using the electrolyte non-random two-liquid (eNRTL) model,» *Fluid Phase Equilibria*, vol. 371, pp. 22-40, 2014.
- [12] M., Von Stackelberg., et H. R., Müller, «On the structure of gas hydrates,» *J. Chem. Phys*, vol. 19, pp. 1319-1320, 1951.
- [13] .. P. B. Dharmawandhana, «PhD Thesis "The measurement of the thermodynamic parameters of the hydrate structure and application of them in the prediction of natural gas hydrates",» Colorado School of Mines, Golden, CO 80401, United States, 1980.
- [14] Y. P. Handa et J. S. Tse, «Thermodynamic properties of empty lattices of structure I and structure II clathrate hydrates,» *J. Phys. Chem*, vol. 90, pp. 5917-5921, 1986.
- [15] A. Danesh, PVT and Phase Behaviour of Petroleum Reservoir fluids, Elsevier Science & Technology Books, 1998.
- [16] A. Thiam, Thesis PhD, Etude des conditions thermodynamiques et cinétiques du procédé de captage de CO<sub>2</sub> par formation d'hydrates de gaz : application au mélange CO<sub>2</sub>-CH<sub>4</sub>, Saint-Etienne: Ecole des mines de Saint-Etienne, 2008.
- [17] John, V.T. and Holder, G.D., *Journal of Physical Chemistry*, vol. 85, n° 113, pp. 1811-1814, 1981.
- [18] Vidal, *Thermodynamic: "Méthodes appliquées au raffinage et au génie chimique"*, Ed. Technip, 1973.
- [19] Jean-Michel Herri, E. Chassefière. «Carbon dioxide, argon, nitrogen and methane clathrate hydrates: Thermodynamic modelling, investigation of their stability in Martian at atmospheric conditions and variability of methane trapping,» *Planetary and Space Science*, vol. 73, n° 11, p. 376–386, 2012.
- [20] Eric Chassefière, Rainer Wieler, Bernard Marty, François Leblanc, «The evolution of Venus: Present state of knowledge and future exploration,» *Planetary and Space Science*, vol. 63–64, pp. 15-23, 2012.